American Mineralogist, Volume 85, pages 613–618, 2000

Structure of a new Al-rich phase, $[K, Na]_{0.9}[Mg, Fe]_2[Mg, Fe, Al, Si]_6O_{12}$, synthesized at 24 GPa

TIBOR GASPARIK,* AKHILESH TRIPATHI, AND JOHN B. PARISE

Center for High Pressure Research and Department of Geosciences, State University of New York at Stony Brook, Stony Brook, New York 11794, U.S.A.

ABSTRACT

A new Al-rich phase, $[K_{0.56}Na_{0.32}][Ca_{0.04}Mg_{1.66}Fe^{2+}_{0.3}][Mg_{0.98}Fe^{3+}_{0.3}Al_{2.62}Si_{2.1}]O_{12}$, was synthesized at 24 GPa, 1700 °C, and its structure was determined by single-crystal X-ray diffraction. The unit cell is hexagonal, space group $P6_3/m$, a = 8.830(1), c = 2.779(1) Å, V = 187.65(5) Å^3, Z = 1, formula weight = 448.62, calculated density = 3.970 g/cm^3. The previously unknown structure consists of alkali- and vacancy-bearing M3 sites in tunnels along c, mostly Mg-bearing linear arrays of trigonal prismatic M2 sites, very unusual for mantle phases, and a framework of edge-linked distorted octahedral M1 sites filled mostly with Al and Si. The observed range of compositional variations and high density suggest complex solid solution behavior at the lower-mantle pressures similar to pyroxenes at the upper-mantle and majorite garnet at the transition-zone pressures. The stability of the Al-rich phase appears to expand to lower Al contents with increasing pressure, suggesting that a chondritic lower mantle could contain up to 24% of the new phase on the molecular basis.

INTRODUCTION

Hutchison (1997) reported the occurrence of a composite inclusion in a diamond from São Luiz, Brazil, consisting of pyroxene with 10.6 wt% of Al_2O_3 in contact with corundum. Since there is no evidence for the stable coexistence of such two minerals, he proposed that pyroxene formed from a $MgSiO_3$ perovskite precursor and thus the composite inclusion represented a lower-mantle assemblage. The stable coexistence of aluminous perovskite with corundum was observed in high-pressure experiments, resulting from the breakdown of pyropic garnet at pressures above 25 GPa (Irifune et al. 1996; Kondo and Yagi 1998). If the composite inclusion is indeed a sample from the lower mantle, it suggests that at least some regions at the top of the lower mantle are substantially enriched in Al_2O_3. In the course of investigating phase relations in such alumina-enriched compositions at the lower-mantle conditions, a new Al-rich phase was synthesized and its structure, determined by single-crystal X-ray diffraction, is reported here.

SYNTHESIS AND ANALYSIS

The synthesis experiment was carried out using a split-sphere anvil apparatus (USSA-2000) and the 10 mm sample assembly (Gasparik, 1990). The starting material was a mixture of synthetic compounds, oxides, and Fe metal (10 mol SiO_2, 8 MgO, 0.2 $CaSiO_3$, 0.4 $NaAlSiO_4$, 0.3 $Na_2Si_2O_5$, 1 $MgCO_3$, 0.5 K_2CO_3, 2Fe°), which was placed in a rhenium sample capsule in contact with a thin layer of synthetic spinel ($MgAl_2O_4$). The experiment was carried out at 24 GPa pressure and temperature of 1700 °C for 2 hours. After the experiment, the sample was mounted in epoxy and polished for microprobe analysis. Wavelength-dispersive chemical analyses (Table 1) were obtained by Cameca electron microprobe using 15 kV accelerating potential, beam current of 10 nA, 10 s counting times to minimize the loss of Na and, as standards, natural enstatite for Mg and Si, grossular for Ca and Al, albite for Na, sanidine for K, and fayalite for Fe.

The sample converted almost completely to perovskite, which was close to pure $MgSiO_3$ in most of the sample, but had a progressively higher Al content as the contact with the spinel layer was approached. An average of the most alumina-rich perovskite compositions from the contact with the spinel layer is given in Table 1 as the "A" analysis. The stoichiometry is consistent with about 60% of Fe being present as Fe^{3+}, despite the effort to minimize Fe^{3+} by introducing all Fe in the starting material as Fe metal. The composition is analogous to garnet with 50 mol% majorite. The new Al-rich phase formed mostly along the contact between the sample and the layer of spinel as relatively large (20–50 µm) blue crystals, which were used for the structure determination (Table 1, B). Smaller blue crystals were also located within the original spinel layer, but their composition was higher in Al and Ca (Table 1, C). Other phases present in the experimental product were K-rich hollandite ($KAlSi_3O_8$), stishovite, and carbonate melt. The Al-rich phase was also synthesized at 22 GPa and 1800 °C, using a different starting material (13.8 mol SiO_2, 9.5 MgO, 7.9 $CaSiO_3$, 4.3 $NaAlSiO_4$, 2 Na_2CO_3, 1 K_2CO_3, 2 Fe° + $MgAl_2O_4$). In this case, the Al-rich phase had a much higher Al content (Table 1, D), and the coexisting phases were garnet and $CaSiO_3$ perovskite.

*E-mail: gasparik@sbmp04.ess.sunysb.edu

TABLE 1. Average microprobe analyses and stoichiometric formulae of perovskite (A) and Al-rich phase (B-D) from high-pressure experiments

	A (7)	B (20)	C (2)	D (4)
	Average microprobe analysis (wt%)			
SiO_2	51.31(50)	28.29(54)	13.06(70)	7.74(60)
Al_2O_3	7.02(15)	29.96(52)	54.16(92)	64.73(80)
FeO	13.17(24)	9.79(25)	5.17(11)	3.62(40)
MgO	31.50(42)	23.42(41)	17.97(46)	15.12(25)
CaO	0.16(4)	0.51(5)	1.48(5)	2.17(22)
Na_2O	0.08(4)	2.21(11)	2.41(1)	2.77(8)
K_2O	0.04(3)	5.96(14)	4.44(14)	3.50(6)
Total	103.28(57)	100.14(76)	98.69(20)	99.65(26)
	Cations per 12 O atoms			
Si	3.497	2.111	0.972	0.567
Al	0.564	2.634	4.751	5.590
Fe^{3+}	0.455	0.295	0.290	0.200
Fe^{2+}	0.259	0.295	0	0
Mg	3.200	2.605	1.993	1.651
Ca	0.012	0.041	0.118	0.171
Na	0.010	0.320	0.348	0.394
K	0.003	0.567	0.422	0.327
Sum	8.000	8.868	8.894	8.900

Notes: Stoichiometric formulae are:
A = $[Mg_{3.24}Fe^{2+}_{0.26}Fe^{3+}_{0.45}Al_{0.05}][Al_{0.5}Si_{3.5}]O_{12}$;
B = $[K_{0.56}Na_{0.32}][Ca_{0.04}Mg_{1.66}Fe^{2+}_{0.3}][Mg_{0.98}Fe^{3+}_{0.3}Al_{2.62}Si_{2.1}]O_{12}$;
C = $[K_{0.42}Na_{0.34}Ca_{0.12}]Mg_2[Fe^{3+}_{0.3}Al_{4.7}Si_{1.0}]O_{12}$; and
D = $[K_{0.32}Na_{0.4}Ca_{0.18}]$
$[Mg_{1.64}Fe^{3+}_{0.2}Al_{0.16}][Al_{5.44}Si_{0.56}]O_{12}$.

STRUCTURE DETERMINATION

The single crystal of the Al-rich phase used for the structure determination was a blue cube, 30 μm on edge, taken from the mount used for microprobe analysis. Single-crystal diffraction data were collected on a Bruker CCD instrument fitted with a graphite monochromator to select Mo$K\alpha$ radiation (λ = 0.71073 Å). The data were consistent with the Laue symmetry 6/m. Unit-cell parameters were determined to be a = 8.830(1), c = 2.7790(6) Å, V = 187.65(5) Å^3, and intensities (1396) were measured to θ = 28.5° for $-11 < h < 11$, $-11 < k < 11$, $-3 < l < 3$. The data, collected with 60 s exposures, were not corrected for the effects of absorption (μ = 2.56 mm^{-1}).

The structure was solved by model building and refined by full-matrix least squares on F^2 using SHELXL (Sheldrick 1986). Three distinct metal sites (M3, M2, M1) were identified, with distinct $(3 + 6)^-$, trigonal prismatic and octahedral coordination, respectively, with oxygen. Refinement of the model began with a simplified chemistry and assuming the following distribution of cations over the three M sites: M3 = $[K_{0.6}Na_{0.4}]$, M2 = Mg, and M1 = Al. Convergence was achieved, and inspection of the M-O distances, with M3-O = 2.6, M2-O = 2.12, and M1-O = 1.90 Å, suggested that the M sites were occupied by alkalis, Mg, and (Al, Si, Mg), respectively. The chemistry of the sites was then adjusted to reflect this assumption. The refinement of the occupancy factors in separate cycles suggested about 10% vacancies in the M1 site, consistent with the chemistry observed by the microprobe analysis (Table 1, B), and that Fe was distributed over the M2 and M1 sites. Because of the differences in the size of these sites, it was assumed that iron in M3 was Fe^{3+}, while that in the trigonal prismatic site was Fe^{2+}. However, the small amount of iron in the sample, the lack of discrimination between the scattering of Al^{3+}, Mg^{2+}, and Si^{4+}, and the similarity in the size of the M2 and M1 sites, made an unambiguous assignment difficult.

The final refinement cycles were carried out by assuming that all chemically analyzed K and Na occupied the M3, and Al and Si were in the M1 site. Fe and Mg were then allowed to occupy both the M2 and M1 sites, with two linear constraints added to maintain the total amount of these elements in the unit cell as $Fe_{0.6}Mg_{2.64}$. The refined amount of iron, $Fe_{0.5}$, is close to the chemically analyzed content (Table 1, B). Final refinement statistics for all 188 unique data were: GOF = 1.053, $R1$ = 0.019, and $wR2$ = 0.047, where $R1$ and $R2$ are the conventional crystallographic "R-value" calculations based on the differences between the observed and calculated F and weighted F^2, respectively. Data in Tables 2 and 3 summarize the refined model, and selected interatomic distances and angles, respectively. Observed and calculated F^2 values are in Table 4.

During the refinement of the anisotropic displacement parameters for the structure of the Al-rich phase, the nature of the M3 site was examined. This site had a pronounced distribution of electron density along [001], with the ratio of U_{33}/U_{11} = 25. A split-site model with isotropic displacement parameters was adopted at no cost to the number of parameters refined. However, both models provided equally good fits to the data.

The structure (Fig. 1) consists of a framework of double chains of edge-linked octahedra running parallel to [001] and corner-linked in the (001) plane. This corner-linkage of octahedral chains is common to the structure of Si-centered octahedra in the stishovite (rutile type) structure and hollandite (e.g., Downs et al. 1995). Rather than forming tunnels surrounded by four walls of edge-linked chains, however, in the structure of the Al-rich phase, there are tunnels of two types. The larger contains K/Na sites surrounded by six columns of edge-linked octahedra, while the second, smaller tunnel is occupied almost exclusively by Mg and is bounded by three double-octahedral chains (Fig. 1).

The M3 site (Fig 2a) contains K, Na, and vacancies, and has an average M-O bond length of 2.58 Å, shorter than the K-

TABLE 2. Fractional atomic coordinates (× 10^4) and equivalent isotropic* and anisotropic‡ displacement parameters (Å^2 × 10^3) for $K_{0.56}Na_{0.32}Ca_{0.04}Mg_{2.64}Fe_{0.6}Al_{2.62}Si_{2.1}O_{12}$

Site	Mult./site symmetry†	x	y	z	U/U_{eq}*	U_{11}‡	U_{22}	U_{33}	U_{12}
M1	6/m	–3447(1)	100(1)	3/4	6(1)	6(1)	6(1)	6(1)	2(1)
M2	$2/\bar{6}$	1/3	2/3	1/4	10(1)	11(1)	11(1)	8(1)	6(1)
M3§	4/3	0	0	8663(7)	10(9)				
O1	6/m	1281(2)	5298(1)	3/4	13(1)	10(1)	13(1)	15(1)	5(1)
O2	6/m	–1116(2)	2052(2)	3/4	18(1)	17(1)	21(1)	19(1)	11(1)

* One third the trace of the orthogonalized U_{ij} tensor for M2, M1, and oxygen sites.
† Space group $P6_3/m$.
‡ $\exp[2\pi^2(U_{11}hha^*a^*....+ 2U_{12}hka^*b^*.....)]$.
§ M3 site slit from ideal site at (0, 0, 1/4) to (0, 0, z); isotropic displacement parameters assumed.

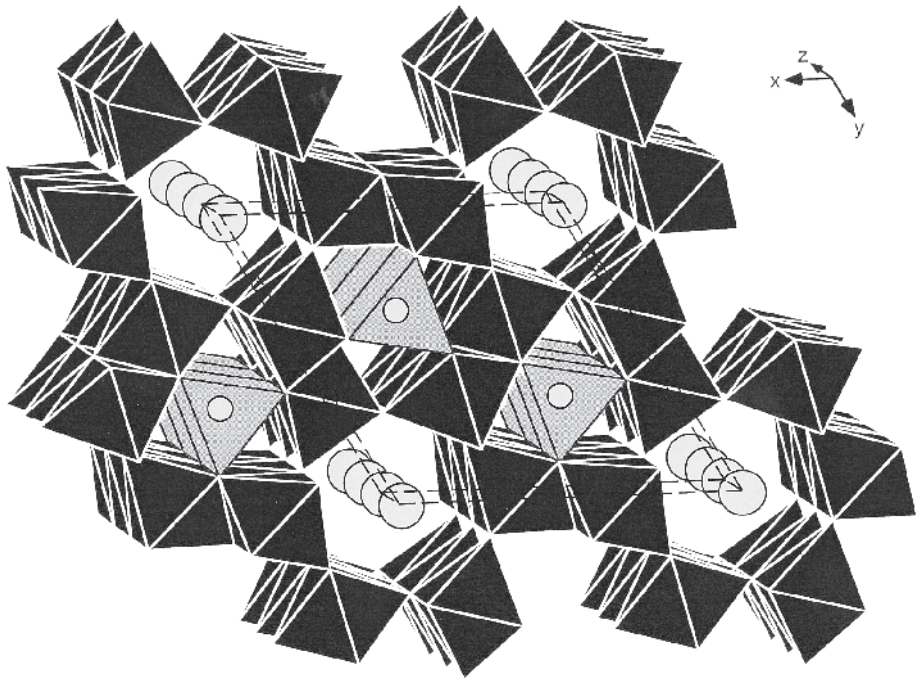

FIGURE 1. Polyhedral representation of the framework structure of Al-rich phase. The structure is composed of double chains of M1-centered octahedra (dark), the M2 sites shown as small open circles at the centers of regular trigonal prisms of O atoms (light), and the M3 sites shown as large circles containing disordered K, Na, and vacancies.

TABLE 3. Selected interatomic distances (Å) and angles (°) for $K_{0.56}Na_{0.32}Ca_{0.04}Mg_{2.64}Fe_{0.6}Al_{2.62}Si_{2.1}O_{12}$

Sites*	Distance	Sites*	Angle
M1-O2§ ×2	1.846(1)	O2§-M1-O2††	97.66(7)
M1-O2	1.913(1)	O2§-M1-O2 ×2	97.37(6)
M1-O1‖	1.942(1)	O2§-M1-O1‖ ×2	94.70(5)
M1-O1§ ×2	1.949(1)	O2-M1-O1‖	161.61(6)
		O2§-M1-O1†† ×2	173.32(6)
M2-O1‡ ×6	2.118(1)	O2††-M1-O1†† ×2	85.39(4)
		O2-M1-O1†† ×2	88.09(4)
M3-M3*	0.646(4)	O1‖-M1-O1†† ×2	79.09(5)
M3-M3†	1.3895(3)	O1††-M1-O1§	90.97(5)
O2-M3* ×3	2.479(8)	O1‡-M2-O1# ×3	82.01(5)
O2-3† ×3	2.68(2)	O1‡-M2-O1** ×6	135.66(2)
		O1#-M2-O1** ×6	81.62(3)

Symmetry transformations used to generate equivalent atoms:
* *x,y,–z*+3/2; † –*x*,–*y*,*z*–1/2; ‡ –*x*+*y*,–*x*+1,*z*; § *x*–*y*,*x*,–*z*+1; ‖ –*x*+*y*–1,–*x*,*z*; # –*x*+*y*,–*x*+1,*z*–1; ** *x,y,z*–1; †† *x*–*y*,*x*,–*z*+2.

O (2.8 Å) distance and longer than the distance Na-O (2.4 Å) expected from the ionic radii of Shannon and Prewitt (1969). A repeated, more detailed collection of a subset of data with 120 s exposure times did not show a superlattice along any axial direction—and especially not along *c*, as might be expected if K and Na were ordered into different sites.

The regular trigonal prismatic coordination found for the M2 site (Fig. 2b) is unusual in high-pressure structures. The M2-O distance (2.12 Å) is slightly shorter than expected (2.26 Å) from the sum of ionic radii (Shannon and Prewitt 1969). The coordination polyhedron for the M1 site (Fig. 2c) is distorted from octahedral in a manner similar to that seen for the edge-linked octahedra in hollandite. Inter-chain repulsive interactions (Fig. 2c) cause M3 to move from the center of the MO_6 octahedron. Distances involving O1 elongate, while those involving O2 shorten to minimize M1-M1 (2.78 Å along and 3.0 Å between chains) and M1-M2 (2.81 Å) repulsion. The O2 atom also coordinates the M3 site. All three M sites provide for a richness of possibilities for the formation of solid solutions and new materials, including replacement of alkalis by hydrogen or coupled substitution of CaAl for NaSi.

IMPLICATIONS

The stoichiometric formula of the new Al-rich phase consistent with the chemical analysis and structure is $[K_{0.56}Na_{0.32}][Ca_{0.04}Mg_{1.66}Fe^{2+}_{0.3}][Mg_{0.98}Fe^{3+}_{0.3}Al_{2.62}Si_{2.1}]O_{12}$. This phase could occur in Al-rich ultramafic compositions potentially present at the top of the lower mantle, as is evident from the composite inclusion described by Hutchison (1997). Indeed, it is quite plausible that this phase will be found in nature as an inclusion in diamond. However, the Al content of an average mantle is too low to allow for the widespread occurrence of such Al-rich phase. Thus, it is useful to evaluate the possibility that the new structure could accommodate compositions with lower Al contents.

The Al-rich phase synthesized at 22 GPa has a substantially higher Al content than observed at 24 GPa, and may represent a composition at the very limit of its stability (Table 1, D). The stoichiometry clearly requires the presence of Ca in the M3 site and confirms the validity of the substitution CaAl = NaSi. An Al-rich phase with higher Al and Ca contents was also present at 24 GPa (Table 1, C), but the Al-rich phase with the highest Si content observed at 24 GPa was not present at 22 GPa. The Al-rich phase coexisted with stishovite at 24 GPa, thus its maximum Mg and Si contents were limited by the co-

TABLE 4. Listing of observed and calculated squared structure factors for the model refined for Al-rich phase, $K_{0.56}Na_{0.32}Ca_{0.04}Mg_{2.64}Fe_{0.6}Al_{2.62}Si_{2.1}O_{12}$, and given in Table 1

h	*k*	*l*	F_o^2	F_c^2	$\sigma(F_o^2)$	*h*	*k*	*l*	F_o^2	F_c^2	$\sigma(F_o^2)$
0	1	0	97.13	93.58	0.97	–9	10	0	0.01	–0.55	1.96
–1	2	0	148.20	151.65	1.37	–8	10	0	15.76	17.80	2.57
0	2	0	67.40	68.96	1.03	–7	10	0	31.25	32.25	2.81
–2	3	0	25.73	25.88	0.95	–6	10	0	49.20	44.57	3.49
–1	3	0	46.91	51.05	1.22	–5	10	0	24.53	23.89	2.36
0	3	0	4255.99	4282.33	11.17	–4	10	0	23.93	21.17	2.25
–3	4	0	40.64	42.99	1.11	–3	10	0	216.16	200.40	6.27
–2	4	0	159.42	163.32	1.83	–2	10	0	79.16	78.72	5.48
–1	4	0	1624.80	1774.24	9.53	–1	10	0	33.82	34.07	3.65
0	4	0	581.94	602.00	4.25	–9	11	0	12.62	14.42	4.79
–4	5	0	13.87	14.28	0.91	–8	11	0	329.79	327.47	16.21
–3	5	0	1.07	1.00	0.82	–7	11	0	121.68	122.58	5.54
–2	5	0	424.99	423.81	5.89	–6	11	0	76.71	79.80	4.51
–1	5	0	54.47	55.68	1.37	–5	11	0	179.85	179.76	5.57
0	5	0	56.20	54.72	1.34	–4	11	0	5.65	0.20	3.55
–5	6	0	312.90	295.12	3.95	–3	11	0	37.11	34.05	3.45
–4	6	0	413.81	397.08	4.57	0	1	1	74.56	71.23	0.99
–3	6	0	3866.91	3827.84	18.54	–1	2	1	905.49	923.84	3.39
–2	6	0	56.13	55.03	1.77	0	2	1	180.63	200.64	1.76
–1	6	0	0.22	0.22	1.01	–2	3	1	1724.02	1781.67	7.33
0	6	0	2728.56	2741.81	11.65	–1	3	1	628.20	651.97	2.89
–6	7	0	25.35	22.06	1.70	0	3	1	193.06	197.39	1.83
–5	7	0	384.90	369.36	8.48	–3	4	1	1265.65	1274.36	7.32
–4	7	0	457.03	413.83	5.09	–2	4	1	2433.56	2452.80	7.71
–3	7	0	53.90	49.82	1.80	–1	4	1	76.98	79.56	1.23
–2	7	0	5.73	4.63	1.22	0	4	1	329.81	332.97	2.69
–1	7	0	421.65	391.27	4.45	–4	5	1	2429.95	2450.10	7.57
0	7	0	61.80	64.10	2.19	–3	5	1	76.94	76.79	1.50
–7	8	0	8.90	10.54	2.07	–2	5	1	204.59	201.78	1.96
–6	8	0	1.54	1.79	1.31	–1	5	1	1351.34	1349.80	5.10
–5	8	0	130.39	125.36	2.93	0	5	1	25.34	25.89	1.09
–4	8	0	0.57	0.85	1.13	–5	6	1	33.12	37.86	1.22
–3	8	0	400.14	383.63	5.44	–4	6	1	417.36	401.58	4.11
–2	8	0	919.33	889.62	10.06	–3	6	1	126.17	125.80	2.01
–1	8	0	44.92	45.81	1.80	–2	6	1	554.63	551.71	4.14
0	8	0	301.67	292.62	5.90	–1	6	1	67.28	67.72	1.59
–8	9	0	31.98	34.26	2.56	0	6	1	101.00	95.49	2.42
–7	9	0	22.53	22.03	2.51	–6	7	1	432.80	418.55	4.38
–6	9	0	829.28	801.67	8.17	–5	7	1	646.27	645.98	6.79
–5	9	0	105.25	105.26	2.94	–4	7	1	47.87	50.23	1.58
–4	9	0	81.32	79.63	2.92	–3	7	1	206.29	209.53	2.81
–3	9	0	1459.22	1415.37	12.29	–2	7	1	154.22	156.82	2.43
–2	9	0	35.86	34.78	2.90	–1	7	1	113.96	112.80	2.30
–1	9	0	46.62	45.92	3.09	0	7	1	177.81	174.65	3.07
0	9	0	1094.70	1117.62	13.65	–7	8	1	535.61	502.59	5.21
–6	8	1	2.43	2.51	1.10	0	6	2	1135.61	1126.45	14.53
–5	8	1	141.39	142.14	2.91	–6	7	2	1.33	–0.10	1.31
–4	8	1	500.31	509.81	6.09	–5	7	2	58.12	63.57	2.26
–3	8	1	23.28	22.73	1.29	–4	7	2	331.55	341.34	4.47
–2	8	1	62.32	65.96	1.91	–3	7	2	89.55	90.12	3.17
–1	8	1	242.52	235.14	3.83	–2	7	2	34.37	35.37	1.92
0	8	1	47.79	51.32	2.00	–1	7	2	316.18	324.43	8.84
–8	9	1	437.21	440.34	5.22	0	7	2	89.35	83.66	3.68
–7	9	1	143.04	145.01	3.72	–7	8	2	30.71	28.73	2.08
–6	9	1	6.59	6.97	1.35	–6	8	2	16.71	16.00	1.93
–5	9	1	71.02	72.98	2.48	–5	8	2	34.36	34.36	2.02
–4	9	1	6.39	5.89	1.27	–4	8	2	11.90	13.89	1.47
–3	9	1	0.11	–0.76	1.08	–3	8	2	108.77	113.29	3.20
–2	9	1	182.38	176.02	3.22	–2	8	2	338.17	360.26	6.82
–1	9	1	108.91	109.86	2.80	–1	8	2	67.29	67.66	3.02
0	9	1	1.07	1.25	1.26	0	8	2	103.06	101.82	3.34
–9	10	1	334.92	384.25	13.28	–8	9	2	3.07	1.11	4.07
–8	10	1	79.52	74.92	2.61	–7	9	2	44.97	43.54	4.73
–7	10	1	154.60	161.07	3.51	–6	9	2	355.95	349.58	8.05
–6	10	1	634.73	645.98	6.98	–5	9	2	20.69	20.97	1.85
–5	10	1	692.98	706.30	13.69	–4	9	2	99.16	106.49	3.06
–4	10	1	29.71	27.31	2.58	–3	9	2	643.01	690.23	8.28
–3	10	1	366.02	373.05	4.97	–2	9	2	52.96	51.17	5.92
–2	10	1	96.03	99.63	2.95	–1	9	2	64.56	60.77	5.22
–1	10	1	61.06	71.41	3.79	–5	10	2	44.46	51.84	5.00
–8	11	1	6.38	8.05	3.67	0	1	3	27.55	29.17	2.14
–7	11	1	124.84	124.65	5.56	–1	2	3	375.56	357.36	5.98
–6	11	1	0.34	–0.52	1.85	0	2	3	3.35	4.00	1.39
–5	11	1	20.42	18.33	2.13	–2	3	3	258.25	253.67	4.74

Table continued on next page

TABLE 4.—*Continued*

h	k	l	F_o^2	F_c^2	$\sigma(F_o^2)$	h	k	l	F_o^2	F_c^2	$\sigma(F_o^2)$
–4	11	1	105.84	105.36	4.96	–1	3	3	63.42	68.59	2.50
–3	11	1	32.77	39.99	4.19	0	3	3	21.34	21.33	1.99
0	0	2	8198.38	7917.55	45.66	–3	4	3	253.18	250.67	4.80
0	1	2	117.64	116.47	2.05	–2	4	3	609.22	580.93	8.95
–1	2	2	137.50	133.90	2.32	–1	4	3	14.38	14.81	1.69
0	2	2	0.49	–0.88	0.88	0	4	3	90.91	93.65	3.36
–2	3	2	4.08	3.64	0.98	–4	5	3	606.06	606.37	8.81
–1	3	2	95.28	95.23	1.88	–3	5	3	14.30	13.44	1.76
0	3	2	1704.15	1705.25	8.00	–2	5	3	48.34	45.55	2.54
–3	4	2	83.94	82.14	2.26	–1	5	3	389.03	385.91	6.45
–2	4	2	1.07	0.75	0.84	0	5	3	5.78	6.72	2.44
–1	4	2	121.69	104.24	2.13	–5	6	3	15.28	12.45	2.57
0	4	2	362.17	356.10	4.24	–4	6	3	95.14	103.86	5.79
–4	5	2	12.59	16.24	1.47	–3	6	3	19.97	19.82	2.00
–3	5	2	18.67	16.85	1.33	–2	6	3	155.44	154.50	4.23
–2	5	2	76.40	76.33	2.55	–1	6	3	5.14	4.66	2.26
–1	5	2	94.16	95.72	2.69	0	6	3	22.77	25.34	3.78
0	5	2	5.40	5.16	1.17						
–5	6	2	60.47	62.19	2.04						
–4	6	2	298.27	303.81	4.70						
–3	6	2	1565.12	1563.89	11.95						
–2	6	2	64.32	65.44	2.25						
–1	6	2	18.11	17.24	1.49						

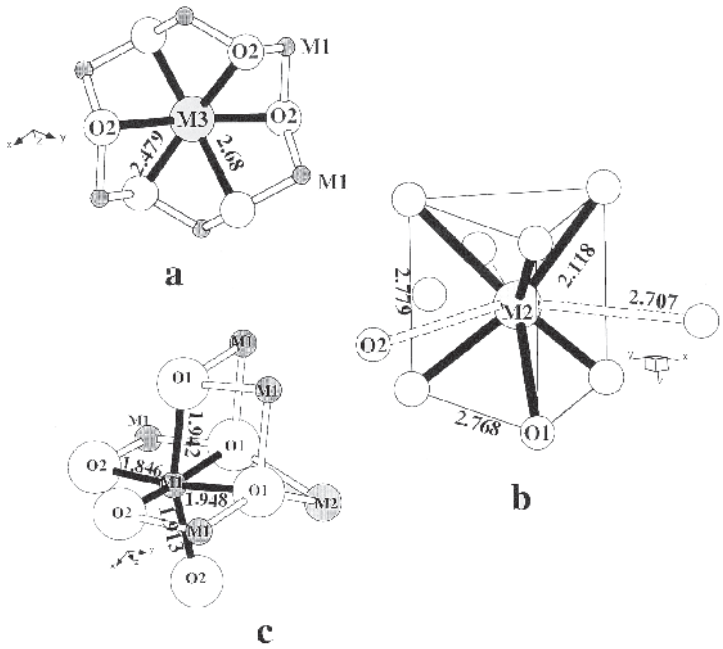

FIGURE 2. The individual coordination environments for the M3 (**a**), M2 (**b**), and M1 (**c**) sites in the structure of Al-rich phase shown in Figure 1.

existing perovskite. Lower Al contents could be possible in the absence of stishovite. These considerations suggest the possibility that an Al-rich phase with lower Al and higher Si than observed could be stable at higher pressures and in the absence of stishovite. It is possible to predict a hypothetical composition with the Al content low enough to allow this phase to be a significant constituent of the lower mantle, with the following formula: $[K, Na]_{0.9}Mg_2[Mg_{1.9}Fe^{3+}_{0.3}Al_{0.8}Si_{3.0}]O_{12}$. The maximum Si content is limited here to 50% of the M1 site occupancy to minimize M1-M1 repulsion resulting from edge sharing. Such forces are evident in the distortion of the M1 octahedra. This composition could accommodate all alkalis present in the mantle, thus replacing $NaAlSiO_4$ in calcium ferrite structure as the most likely host for Na in the lower mantle (Yamada et al. 1983; Gasparik 1992, 1997). If this is the case, a chondritic lower mantle could contain up to 24% of such Al-rich phase on the molecular basis, only second in abundance after $MgSiO_3$ perovskite.

Unknown Al-rich phases forming by the breakdown of garnet at pressures higher than 24 GPa have been reported in a number of studies (Ito and Takahashi 1987; Ahmed-Zaïd and Madon 1995; Funamori et al. 1997; Fujino et al. 1998; Kondo and Yagi 1998; Oguri et al. 1998). None of these studies were carried out with compositions containing alkalis, which appear

to be essential cations in our Al-rich phase. However, the Al-rich phase reported by Irifune and Ringwood (1993) contained alkalis and could have the structure described in this study, although its composition was different. It is also possible that the new structure reported here could be stabilized even in the absence of alkalis, for example with Ca in the M3 site, which would further increase the importance of this phase in the lower mantle. In addition, other minor elements, such as Ti, Cr, Mn, etc., are more likely accommodated in the Al-rich phase than in $MgSiO_3$ perovskite. Thus the Al-rich phase apparently exhibits complex solid solution behavior in the lower mantle similar to pyroxenes in the upper mantle and majorite garnet in the transition zone. Curiously, although in the upper mantle this complex solid solution behavior is limited to minerals with higher silica contents, it becomes important in a silica undersaturated phase in the lower mantle.

Acknowledgments

This study was partially funded by the National Science Foundation grant EAR-9710158 to T.G. J.B.P. is grateful for the support of the NSF (DMR-9713375 and EAR-9724501) grants for the purchase of the X-ray equipment used in this investigation. The high-pressure experiments reported in this paper were performed in the Stony Brook High Pressure Laboratory, which is jointly supported by the National Science Foundation Science and Technology Center for High Pressure Research (EAR-8920239) and the State University of New York at Stony Brook.

References cited

Ahmed-Zaïd, I. and Madon, M. (1995) Electron microscopy of high-pressure phases synthesized from natural garnets in a diamond anvil cell: Implications for the mineralogy of the lower mantle. Earth and Planetary Science Letters, 129, 233–247.

Downs, R.T., Hazen, R.M., Finger, L.W., and Gasparik, T. (1995) Crystal chemistry of lead aluminosilicate hollandite: A new high-pressure synthetic phase with octahedral Si. American Mineralogist, 80, 937–940.

Fujino, K., Miyajima, N., Yagi, T., Kondo, T., and Funamori, N. (1998) Analytical electron microscopy of the garnet-perovskite transformation in a laser-heated diamond anvil cell. In M.H. Manghnani and T. Yagi, Eds., Properties of Earth and Planetary Materials at High Pressure and Temperature, Geophysical Monograph 101, p. 409– 417. American Geophysical Union, Washington.

Funamori, N., Yagi, T., Miyajima, N., and Fujino, K. (1997) Transformation in garnet from orthorhombic perovskite to $LiNbO_3$ phase on release of pressure. Science, 275, 513–515.

Gasparik, T. (1990) Phase relations in the transition zone. Journal of Geophysical Research, 95, 15751–15769.

——(1992) Enstatite-jadeite join and its role in the Earth's mantle. Contributions to Mineralogy and Petrology, 111, 283–298.

——(1997) A model for the layered upper mantle. Physics of the Earth and Planetary Interiors, 100, 197–212.

Hutchison, M.T. (1997) The constitution of the deep transition zone and lower mantle shown by diamonds and their inclusions. Ph.D. Thesis, University of Edinburgh.

Irifune, T. and Ringwood, A. E. (1993) Phase transformations in subducted oceanic crust and buoyancy relationships at depths of 600–800 km in the mantle. Earth and Planetary Science Letters, 117, 101–110.

Irifune, T., Koizumi, T., and Ando, J. (1996) An experimental study of the garnet-perovskite transformation in the system $MgSiO_3$-$Mg_3Al_2Si_3O_{12}$. Physics of the Earth and Planetary Interiors, 96, 147–157.

Ito, E. and Takahashi, E. (1987) Ultrahigh-pressure phase transformations and the constitution of the deep mantle. In M.H. Manghnani and Y. Syono, Eds., High-Pressure Research in Mineral Physics, Geophysical Monograph 39, p. 221–229, American Geophysical Union, Washington.

Kondo, T. and Yagi, T. (1998) Phase transition of pyrope garnet under lower mantle conditions. In M.H. Manghnani and T. Yagi, Eds., Properties of Earth and Planetary Materials at High Pressure and Temperature, Geophysical Monograph 101, p. 419– 427. American Geophysical Union, Washington.

Oguri, K., Funamori, N., Uchida, T., Yagi, T., Miyajima, N., and Fujino, K. (1998) High- pressure and high-temperature in situ X-ray diffraction study of natural garnet $(Mg_{0.72}Fe_{0.17}Ca_{0.11})_3Al_2Si_3O_{12}$ up to 32 GPa and 2000 K using MA8-type apparatus. The Review of High Pressure Science and Technology, 7, 59–61.

Shannon, R.D. and Prewitt, C.T. (1969) Effective ionic radii in oxides and fluorides. Acta Crystallographica, B25, 925–946.

Sheldrick, G.M. (1986) SHELXS-86. Institut für Anorganische Chemie der Universität, Göttingen, Germany.

Yamada, H., Matsui, Y., and Ito, E. (1983) Crystal-chemical characterization of $NaAlSiO_4$ with the $CaFe_2O_4$ structure. Mineralogical Magazine, 47, 177–181.

Manuscript received May 5, 1999
Manuscript accepted December 20, 1999
Paper handled by Simon A.T. Redfern